Elastic-stiffness distribution on polycrystalline Cu studied by resonance ultrasound microscopy: Young's modulus microscopy

H. Ogi,* M. Hirao, and T. Tada
Graduate School of Engineering Science, Osaka University, Toyonaka, Osaka 560-8531, Japan

J. Tian
Institute of Crustal Dynamics, Chinese Earthquake Administration, Beijing 100085, China
(Received 15 March 2006; published 9 May 2006)

We study an elastic-constant distribution on a polycrystalline Cu using resonant ultrasound microscopy with a wireless-electrodeless langasite oscillator, which we originally developed for absolute quantitative determination of local stiffness of a material. We formulate the relationship between the resonance frequency of the oscillator and material's elastic constants. Our microscopy results on each crystallite agree with those from electron-backscattering-pattern measurements except for some small grains. A softening is observed on grain boundaries, partially explaining softened small grains.

DOI: 10.1103/PhysRevB.73.174107 PACS number(s): 62.20.Dc, 46.40.Ff, 61.72.Mm, 68.37.−d

I. INTRODUCTION

Material's elastic constants reflects strengths of interatomic bond stretching and bond bending. They provide important knowledge of the solid's thermodynamic features, such as the Debye temperature and the Grünisen parameter.[1,2] Macroscopically, the elastic constants reflect defects through elastic softening and elastic anisotropy.[3–5] Thus, local elastic constants serve two purposes; (i) the study of microscale and nanoscale solid-state physics, and (ii) a nondestructive evaluation of solids with damages.

An estimation of local elastic properties has become possible through atomic-force-acoustic microscopy.[6–8] This method estimates the effective stiffness in a local area from the resonance frequency of an atomic-force-microscopy cantilever contacting the material with a needle tip's free end. It achieves a high-resolution microscopy, but it is limited to relative stiffness microscopy because the vibrating cantilever contacts not only the specimen but also the attached piezoelectric oscillator and the fixed end. The key for absolute quantitative stiffness microscopy is that the oscillator vibration must be isolated from any other acoustical contacts on the oscillator's surfaces except the specimen contact. Neither wire nor electrode must be involved.

Recently, we developed a wireless-electrodeless stiffness microscopy with a monocrystal langasite oscillator.[9,10] It showed great potential for evaluating the local elastic constant, but remained providing relative values because of the low sensitivity of the frequency to the modulus and unfavorable contacts between the crystal's side faces and the surrounding fixture walls, which prohibited extracting the frequency change caused only by the contact with the specimen.

Here, we further develop an oscillator for realizing a much higher sensitivity and making it completely isolated, and we propose a vibrational analysis by incorporating the contact between anisotropic materials to calculate the materials stiffness from the measured frequency. The microscopy method is applied to study the elastic-stiffness distribution on polycrystalline copper and it finds out softened crystallites.

II. MEASUREMENT

Our homebuilt microscopy consists of a monocrystal langasite ($La_3Ga_5SiO_{14}$) oscillator, diamond tip (12-μm diameter) attached to the bottom surface of the crystal, the surrounding solenoid-coil antenna, epoxy fixture for the crystal, and an *XYZ* stage on which a specimen is put. All the components are placed in a vacuum chamber ($\sim$1 Pa) to avoid acoustic noise. Langasite shows low temperature derivatives of the elastic constants, of the order of 10^{-6}–10^{-5}, requiring no temperature controlling. It also shows high piezoelectricity, allowing us to generate and detect vibrations contactlessly by the solenoid-coil antenna.[11] The langasite crystal is an oriented rectangular parallelepiped, showing the cross-section area of 2×2 mm^2 and the length of 7 mm. The crystal's twofold axis (*X* axis) is selected along the longitudinal direction. When a sinusoidal current is applied to the solenoid coil, a quasistatic electric field (nonrotational component) (E_x) is generated along the vertical direction, causing the principal stresses $-e_{11}E_x$ along the *X* direction and $e_{11}E_x$ along the *Y* direction via the converse piezoelectric effect. e_{11}denotes a piezoelectric coefficient of materials showing a 32-point-group symmetry. Thus, this setup causes breathing vibrations (A_g vibration group[11,12]). The same solenoid coil detects the vibrational amplitudes through the piezoelectric effect and a frequency scan yields the resonance spectrum, requiring neither wires nor electrodes on the oscillator surfaces.

We used the fundamental mode of the breathing vibration (A_g-1) because it has nodal lines at the center on the side faces and an antinode point at the center of the bottom surface to achieve a high sensitivity. (The sensitivity to the modulus increased by a factor of 50 comparing our previous oscillator in Refs. 9 and 10.) The vibrational amplitude distribution was confirmed by the laser-Doppler interferom-

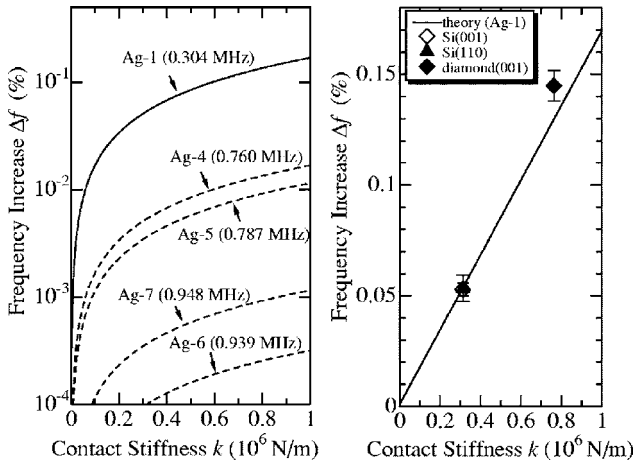

FIG. 1. Relationships between the contact stiffness and the resonance frequencies of the A_g vibration group (left) and a comparison of the calculated frequency shift with measurements (right) for the A_g-1 mode. No fitting parameters are involved in the calculation of the contact stiffness and resonance frequencies.

eter[13] and we supported the langasite oscillator by the epoxy fixture exactly at the nodal lines on the side faces, giving little influence on the vibration.

III. VIBRATIONAL ANALYSIS

This isolated vibrational system has made it possible to determine the local modulus quantitatively. The contact between the tip and specimen is equivalent to an elastic spring with the contact stiffness k.[14] The resonance frequency is calculated by the Lagrangian minimization with the Rayleigh-Ritz method. The system Lagrangian consists of the elastic strain energy, electromechanical coupling energy, electrostatic energy of the langasite crystal,[11,12,15] kinetic energy of the tip, and the elastic-spring energy at the tip-specimen contact interface.[10] No gripping effect is involved. Because of the isolated vibrational system, we require only the crystal's dimensions, elastic and piezoelectric coefficients, and the mass of the tip, which are all unambiguously measurable. The displacements and electric potential are approximately expressed by a combination of many basis functions of Legendre polynomials (Rayleigh-Ritz approach).[11,12,15] Calculated frequencies agreed with those measured within 0.1% for first 40 modes: One would never obtain such an excellent agreement between measured and calculated frequencies in the use of the cantilever-type oscillator because of ambiguous parameters.

Figure 1 shows the sensitivity of A_g-group resonance frequencies to the contact stiffness k; the highest sensitivity of the fundamental mode (A_g-1) is associated with the large out-of-plane amplitude at the contacting point. Its sensitivity is actually very high because our microscopy determines the resonance frequency within the error limit of 2×10^{-5}. When we find a relationship between the contact stiffness k and the effective elastic constant of the material, we can determine the effective stiffness only from the resonance frequency. We propose this relationship following Willis and Swanson: Willis[16] formulated contact features between two anisotropic bodies using the Fourier transform, and Swanson[17] calculated the indentation depth δ using Willis's approach in the case of the contact with orthorhombic materials by $\delta=3F_0I_0/(8a)$, where F_0 is the biasing force normal to the surface and a denotes the average contact radius given by $a=\sqrt[3]{3RF_0I_1/4}$. Here, R denotes the tip radius. I_0 and I_1 are given by integrating the Green function $\hat{G}$ for a point-force indentation, which depends on the elastic constants of the specimen:

$$I_0=\sum_{i=1}^{2}\int_0^{2\pi}\hat{G}_i(\epsilon\eta_x,\eta_y)d\theta,\quad I_1=\sum_{i=1}^{2}\int_0^{2\pi}\hat{G}_i(\epsilon\eta_x,\eta_y)\eta_x^2d\theta.$$

Here $i=1$ represents quantities of the tip and $i=2$ those of the specimen. $\eta_x=\cos\theta$ and $\eta_y=\sin\theta$; θ denotes the angle of the polar-coordinate system on the contact-interface plane. ϵ is the ratio between the major and minor axes of the ellipsoid of the contact interface; obtained by an iterative calculation, it equals approximately unity.

The harmonic oscillation of the oscillator causes harmonic perturbation in the applied force and the total force will be of the form $F_0+\Delta F$ at the contact interface. We assume $|\Delta F|\ll|F_0|$ to obtain $\Delta\delta\approx\Delta F\sqrt[3]{I_0^3/(48F_0RI_1)}$. Thus, we derive the contact stiffness k for the contact between two orthorhombic materials:

$$k=\sqrt[3]{48F_0RI_1/I_0^3}. \tag{1}$$

Equation (1) applies when the two orthogonal axes of the material are parallel to the contact interface. In Fig. 1, we plot the experimental Δf versus k for the contacts with (001) and (110) faces of monocrystal silicon wafers and the (001) face of monocrystal diamond. Remarkably, they agree with the theoretical calculation regardless of the absence of fitting parameters. This demonstrates that isolation of the oscillator is the key of the quantitative microscopy.

Our goal is to determine the effective modulus of the specimen only from the resonance-frequency shift of the oscillator. A classical Hertzian theory relates the effective modulus E^* to the contact stiffness k through $E^*=\sqrt{k^3/(6RF_0)}$ in the case of the contact of two isotropic bodies,[18] where E^* is given by

$$E^*=[(1-\nu_t^2)/E_t+(1-\nu_s^2)/E_s]^{-1}. \tag{2}$$

Here, ν and E denote Poisson's ratio and Young's modulus, and subscripts t and s denote the tip and specimen, respectively. Similarly, we define the effective modulus for the contact between the anisotropic bodies by

$$E^*=\sqrt{8I_1/I_0^3}. \tag{3}$$

Thus, the effective normal Young's modulus of the specimen E_s is given by Eqs. (2) and (3).

IV. RESULTS AND DISCUSSION

Using our original microscopy, we measure the stiffness distribution on the polycrystalline copper and compare the result with that obtained by the electron-backscattering-pat-

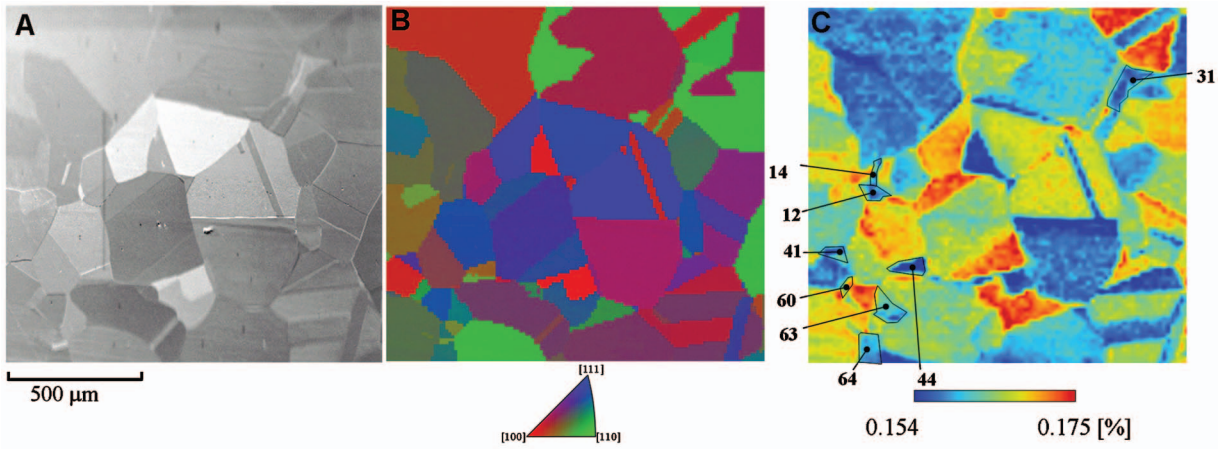

FIG. 2. (Color) Scanning-electron-microscopy image (a), crystallographic-orientation image for the normal direction to the surface measured by the EBSP method (b), and resonance-frequency image (c). F_0=0.019 N. Numbered grains indicate smaller stiffnesses than those estimated by grain orientations.

tern (EBSP) measurement. The studied material was an oxygen-free high-conductivity copper. Purity exceeded 99.95%. The EBSP measurement was carried out before the elastic-stiffness mapping. After annealing at 800 °C for 2 h, the surface layer (~30 μm thick) was removed chemically to obtain a nonstrained surface, and Kikuchi patterns were obtained for every 7 μm. Figures 2(a) and 2(b) compare an image obtained by the scanning electron microscopy with a crystallographic orientation image determined by the EBSP measurement. We measured the resonance frequency for every 5 μm on the same area examined by EBSP. At each measuring point, the change of the resonance frequency between before and after making contact was recorded. Figure 2(c) shows the resonance-frequency image, showing clearly the difference of the elastic stiffness depending on the crystallite orientation. Even within a single grain, the resonance frequency is nonuniform, indicating elastic-constant distribution.

Because Eq. (3) applies only to orthorhombic materials, we averaged the elastic-stiffness tensor over the rotational angle in the surface plane at each point using Hill's averaging method[4] and crystallographic orientations determined by EBSP measurements: The averaged elastic-stiffness tensor $\langle C_{ijkl} \rangle$ is given by

$$\langle C_{ijkl} \rangle = \frac{1}{2}\left\{ \frac{1}{2\pi}\int_0^{2\pi} C_{ijkl}(\theta)d\theta + \left(\frac{1}{2\pi}\int_0^{2\pi} s_{ijkl}(\theta)d\theta \right)^{-1} \right\}. \tag{4}$$

Here, s_{ijkl} denotes the elastic compliance tensor. This procedure yields transverse-isotropic (hexagonal) elastic symmetry to accept the above analysis. Figure 3 compares the effective normal Young modulus determined by the observed frequency shift and that calculated by the EBSP measurement for individual grains; there were 74 grains in the scanned area and we numbered them. The effective Young modulus determined by our elastic microscopy failed to show a perfect agreement with that by EBSP because of the simplification of the contact-stiffness calculation in order to accept the Willis-Swanson analysis. However, they show a good correlation as shown by the solid line; this is remarkable because no fitting parameters are included in the calculation of the effective modulus from the resonance frequency.

We note that some grains show smaller stiffnesses than those estimated by EBSP measurements. These are smaller grains as labeled in Figs. 2(c) and 3. We attribute this discrepancy to two factors. First, elastic softening at the grain boundaries is caused by lattice distortion. Polycrystalline materials tend to show smaller elastic constants than those

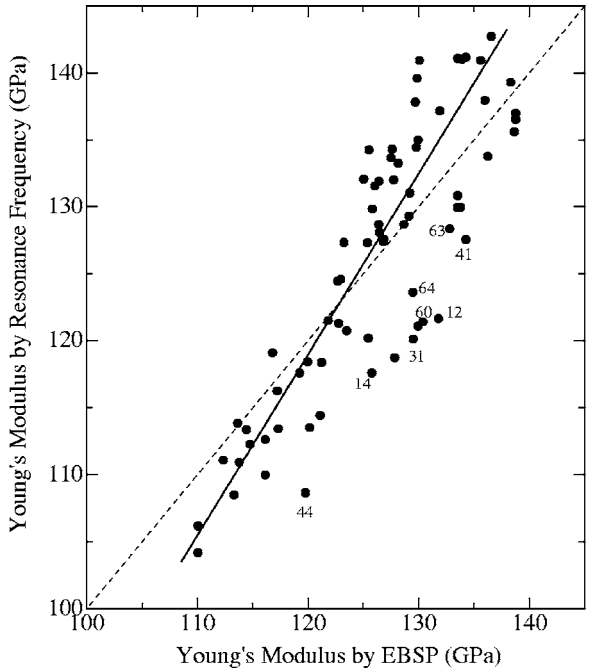

FIG. 3. A comparison between the effective normal Young modulus determined by the resonance frequency and that by the EBSP measurement. The slope of the broken line is 1. The solid line indicates the strong correlation between them. Numbered grains correspond to those in Fig. 2(c).

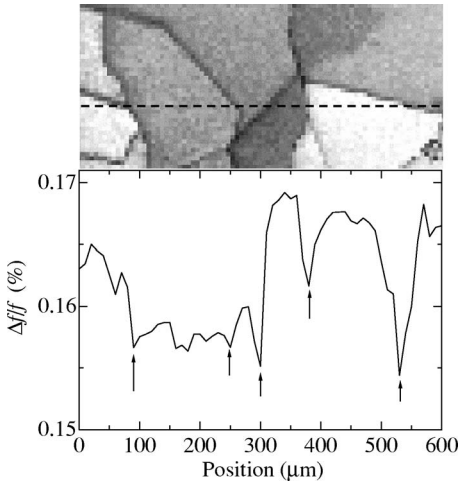

FIG. 4. An image of the quality factor in the EBSP measurement (top) and the line trace of the resonance-frequency change along the broken line shown in the image (bottom). Arrows indicate grain boundaries.

for an aggregate computed from elastic constants of corresponding monocrystals.[19] The volume fraction of such softened regions near grain boundaries increases in a small grain. Figure 4 shows a linear trace of the resonance frequency along the horizontal broken line, which indicates the stiffness decrease near grain boundaries. The top figure in Fig. 4 shows a low quality factor of EBSP at the grain boundaries, indicating low crystallinity.

Second is a small-grain elastic softening caused by an elastic strain (or lattice anharmonicity). Phillips *et al.*[20] found by using x-ray microdiffraction measurements[21] that elastic strains in some small grains (not all) are much larger than in large grains in Al-Cu polycrystalline thin films: The maximum resolved shear strain reaches 0.6%. In small grains, less plastic deformation occurs because dislocations cannot move freely because of the grain-boundary back stress. The modulus decrement is estimated roughly to be 3–8% from the correlation line in Fig. 3. We estimate the elastic strain that may cause this decrement from the temperature dependence of the elastic constants. Copper's Young's modulus is 135.7 GPa at 100 K and 127.0 GPa at 300 K;[22] it decreases by 6.4% by the 200-K temperature increase, corresponding to the 1% volume change, assuming the constant thermal expansion coefficient of 18×10^{-6} K^{-1}. Thus, to explain a decrease of Young's modulus in small grains, we expect about 0.3% uniaxial strain. Young's modulus is highly affected by the shear modulus because it is about eight times as sensitive to the shear modulus as to the bulk modulus. Zener[23] showed that the variation of the shear modulus with the strain energy caused by thermal vibrations (thermal expansion) is identical with that caused by the strain energy due to residual stresses. Therefore, considering the large residual resolved shear strain observed in an Au-Cu alloy,[20] decrease of Young's modulus by several percent is possible. Thus, smaller grains may include residual strains large enough to change the elastic constant, approximately by 10^{-2}. The stiffness distribution within a single grain can, therefore, be interpreted as arising from the residual-strain distribution.

V. CONCLUSION

We developed a microscopy method for a quantitative determination of effective elastic stiffnesses in a microscale region. The relationship between the resonance-frequency change and the material's anisotropic elastic constants was formulated. Its correctness and usefulness were demonstrated by comparing the determined modulus to that predicted by EBSP measurements for a polycrystalline copper. This homemade microscopy detected elastic softening grain boundaries and softened small grains, which were attributed to a lattice distortion due to a larger residual strain in small grains.

ACKNOWLEDGMENT

This study was supported by the Industrial Technology Research Grant Program in 2004 from the New Energy and Industrial Technology Development Organization (NEDO).

*Electronic address: ogi@me.es.osaka-u.ac.jp

[1] O. Anderson, *Equations of State of Solids for Geophysics and Ceramic Science* (Oxford University Press, New York, 1995).
[2] V. Keppens and A. Migliori, Elastic Properties and Thermodynamics, in *Handbook of Elastic Properties of Solids, Liquids and Gases*, edited by M. Levy, H. Bass, and R. Stern (Academic, San Diego, 2001), Chap. 12, pp. 173–184.
[3] H. Ogi, G. Shimoike, M. Hirao, K. Takashima, and Y. Higo, J. Appl. Phys. **91**, 4857 (2002).
[4] N. Nakamura, H. Ogi, and M. Hirao, Acta Mater. **52**, 765 (2004).
[5] H. Ogi, N. Nakamura, H. Tanei, R. Ikeda, M. Hirao, and M. Takemoto, Appl. Phys. Lett. **86**, 231904 (2005).
[6] K. Yamanaka, H. Ogiso, and O. Kolosov, Appl. Phys. Lett. **64**, 178 (1994).
[7] U. Rabe and W. Arnold, Appl. Phys. Lett. **64**, 1493 (1994).
[8] K. Yamanaka, T. Tsuji, A. Noguchi, T. Koike, and T. Mihara, Rev. Sci. Instrum. **71**, 2403 (2000).
[9] H. Ogi, J. Tian, T. Tada, and M. Hirao, Appl. Phys. Lett. **83**, 464 (2003).
[10] H. Ogi, T. Tada, J. Tian, and M. Hirao, Jpn. J. Appl. Phys., Part 1 **44**, 4381 (2005).
[11] H. Ogi, N. Nakamura, K. Sato, M. Hirao, and S. Uda, IEEE Trans. Ultrason. Ferroelectr. Freq. Control **50**, 553 (2003).
[12] I. Ohno, Phys. Chem. Miner. **17**, 371 (1990).
[13] H. Ogi, K. Sato, T. Asada, and M. Hirao, J. Acoust. Soc. Am. **112**, 2553 (2002).
[14] K. Johnson, *Contact Mechanics* (Cambridge University Press, Cambridge, 1985).
[15] H. Ogi, Y. Kawasaki, M. Hirao, and H. Ledbetter, J. Appl. Phys. **92**, 2451 (2002).
[16] J. Willis, J. Mech. Phys. Solids **14**, 163 (1966).
[17] S. Swanson, Int. J. Solids Struct. **41**, 1945 (2004).

[18] G. Yaralioglu, F. Degertekin, K. Crozier, and C. Quate, J. Appl. Phys. **87**, 7491 (2000).

[19] H. Ogi, S. Kai, H. Ledbetter, R. Tarumi, M. Hirao, and K. Takashima, Acta Mater. **52**, 2075 (2004).

[20] M. A. Phillips, R. Spolenak, N. Tamura, W. L. Brown, A. A. MacDowell, R. S. Celestre, H. A. Padmore, B. W. Batterman, E. Arzt, and J. R. Patel, Microelectron. Eng. **75**, 117 (2004).

[21] R. Spolenak, W. L. Brown, N. Tamura, A. A. MacDowell, R. S. Celestre, H. A. Padmore, B. Valek, J. C. Bravman, T. Marieb, H. Fujimoto, B. W. Batterman, and J. R. Patel, Phys. Rev. Lett. **90**, 096102 (2003).

[22] W. C. Overton, Jr. and J. Gaffney, Phys. Rev. **98**, 969 (1955).

[23] C. Zener, Acta Crystallogr. **2**, 163 (1949). See EPAPS Document No. E-PRBMDO-73-051617 for details of the measurement setup and elastic-anelastic images obtained for other material. This document can be reached via a direct link in the online article's HTML reference section or via the EPAPS homepage (http://www.aip.org/pubservs/epaps.html).